

**Airflow distortion at instrument sites on the
RV *Knorr***

B. I. Moat & M. J. Yelland

1998

James Rennell Division for Ocean Circulation and Climate
Southampton Oceanography Centre
University of Southampton
Waterfront Campus
European Way
Southampton
Hants SO14 3ZH
UK

Tel: +44 (0)023 8059 6406
Fax: +44 (0)023 8059 6204
Email: Ben.Moat@soc.soton.ac.uk

AIRFLOW DISTORTION AT INSTRUMENT SITES ON THE RV KNORR

1. Introduction	1
2. Description of the RV Knorr model (VECTIS model run 3.2/7)	1
3. The air flow at the lattice tower instrument sites.	2
3.a The instrument locations.	2
3.b The vertical displacement of the flow.	2
3.c The free stream velocity	4
3.d The effect of flow distortion on the wind speed.	4
4. The air flow at the IMET foremast and bowmast instrument sites.	6
4.a The IMET instrument locations	6
4.b The vertical displacement and velocity error	6
5. Summary	8
6. Acknowledgements	10
7. References	10
8. Figures	12
9. Appendix	25

AIRFLOW DISTORTION AT INSTRUMENT SITES ON THE RV KNORR

B. I. Moat and M. J. Yelland

September 1998

1. Introduction

This report describes an investigation of the air flow around the RV Knorr using the Computational Fluid Dynamics software package "VECTIS" to simulate a flow of air directly over the bows of the ship. Section 2 gives a brief description of the model. This work was undertaken at the request of researchers from the Bedford Institute of Oceanography (BIO), the National Oceanic and Atmospheric Administration (NOAA) and Kiel University who had used the ship to carry meteorological instrumentation on a purpose-built mast (the "lattice tower") during an experiment in the Labrador Sea in the winter of 1997.

One advantage of the VECTIS software is the ability to vary the computational mesh density; this allows regions of particular interest to be modelled using a much higher resolution than that employed elsewhere in the model. In the case of the Knorr, the highest mesh density was located around the instrument sites on the lattice tower. In Section 3 the distortion of the air flow to these instrument sites is examined, and the vertical displacement of the flow and the percentage wind speed error is calculated for each site. Section 4 describes the flow at the separate IMET instrument sites on the ship's foremast and bowmast. The mesh resolution at the IMET sites is not as great as that around the lattice tower since data for the IMET sites were requested towards the end of the study. The results are summarised and discussed in Section 5.

2. Description of the RV Knorr model (VECTIS model run 3.2/7)

Figure 1 shows the modelled geometry of the RV Knorr. The solid circles indicate the position of the three main instrument sites; the top of the lattice tower, the IMET instrument site on the foremast and the IMET instrument site on the bowmast. The ship model was enclosed in the centre of a "wind tunnel", or computational volume, which was 600 m long ($-300 < x < 300$), 300 m wide ($-150 < z < 150$) and 150 m high ($0 < y < 150$) (see Moat and Yelland, 1998). The centreline of the ship was parallel to the x-axis at $z=0$. A logarithmic wind profile was specified at the inlet of the wind tunnel, with a 10 metre wind speed of 15 m/s. While the computational solver was running the flow in the tunnel was monitored at seven locations towards one side of the tunnel and at one anemometer location, indicated schematically in Figure 2. The data from these monitoring positions showed that the solution had converged after about 6800 time steps. Figure 3 shows the velocity of the flow for the last 300 time steps, by which point all values were constant to the third significant figure. A post-processing file was then written for the extraction of data throughout the computational volume. Illustrations of the output are contained in the Appendix. A complete description of the procedures used can be found in Moat et al. (1996).

The flow in the tunnel was examined to ensure that freestream conditions existed at the sides and ends of the tunnel, i.e. that the presence of the ship did not cause significant blockage to the flow in these regions. Figure 4a shows the variation of velocity along the tunnel from $x=-200$ m to $x=+200$ m, at heights of 10, 20, 30 and 50 m, on a plane at $z = 100$ m, i.e. towards one side of the tunnel. Equivalent data were also extracted from the opposite side of the tunnel, at $z = -100$ m, which gave identical results to those shown. The central section of the tunnel only is shown in more detail in Figure 4b, which displays velocity data directly abeam of the ship. This shows a change in the freestream velocity of about 0.10 m/s at a height of 10 m and 0.04 m/s at a height of 20 m. These small changes indicate that the ship caused minimal blockage to the flow at the sides of the tunnel. However, since the changes are not zero, the free stream velocity for a particular instrument site is estimated using the vertical profile of velocity 100 m directly abeam of the instrument site, rather than the profiles at the inlet or outlet of the tunnel.

3. The air flow at the lattice tower instrument sites.

3.a The instrument locations.

The locations of the four anemometers and the fast response temperature sensor on the lattice tower are shown in Figure 5. These instruments were all mounted on the lattice tower sited in the bows of the ship. It must be noted that the tower itself was not modelled since its open lattice construction was too fine to be resolved properly in the model (see Moat and Yelland, 1998). However, the positions of the instruments were given relative to the top of the tower, and are shown in this fashion in the Figure. Moat and Yelland indicated the coordinates of the top of the tower as $x=35.52$, $y=18.22$, $z=1.57$. Subsequent discussion with the researchers involved suggested that these coordinates should be $x=34.77$, $y=17.73$ and $z=1.06$ i.e. that the tower was slightly shorter and located a little further aft than originally thought. These latter coordinates were used for the analysis described below.

In the VECTIS model co-ordinates system, the instrument positions ("P" in the following tables) are;

BIO sonic anemometer	$x = 34.77$ m	y (height) = 18.40 m	$z = 2.21$ m
BIO Young anemometer	$x = 34.77$ m	y (height) = 18.66 m	$z = 1.79$ m
NOAA sonic anemometer	$x = 35.17$ m	y (height) = 18.78 m	$z = 1.06$ m
Kiel sonic anemometer	$x = 34.77$ m	y (height) = 18.46 m	$z = 0.46$ m
Fast temperature sensor	$x = 34.77$ m	y (height) = 17.90 m	$z = 0.06$ m

3.b The vertical displacement of the flow.

To calculate the vertical displacement of the flow reaching the instrument a streamline is traced from the inlet of the tunnel to the instrument site (see Figure A5 in the Appendix). Table 1 gives the co-ordinates of; "P" the BIO sonic anemometer site, "Pstream" which is the point on the streamline closest to the anemometer, and the position of the start of the

streamline "P_{origin}". It can be seen that the streamline is displaced vertically by 0.74 m by the time it reaches the approximate position of the anemometer site. Tables 2 to 5 give the equivalent information for the BIO Young, NOAA sonic, Kiel sonic and Fast temperature sensor sites respectively. In most cases the streamlines pass within a few centimetres of the instrument location in the x and y directions, but miss by up to 47 cm in the z (port-starboard) direction for the Kiel sonic. This is because the streamline originates from a cell far upstream of the ship, where the cell size is relatively large. A vertical section (constant z) of data is viewed, and the x and y coordinates of the origin of the streamline are adjusted until the streamline passes through the anemometer site, but no such fine adjustment in the z direction is possible. This inaccuracy in the location of the streamlines could cause errors in the calculation of the vertical displacements of up to 10 cm.

Examination of the streamlines intersecting the lattice tower sites showed that the vertical displacement began about 35 m upstream of the instruments, and that two thirds of the displacement occurred in the last 15 m. For a wind speed of about 15 m/s, this implies that it takes about 2 seconds for the flow to be displaced vertically from its original height to the height of the anemometers. This should be borne in mind if data from the instruments is used to estimate the surface fluxes using the inertial dissipation method (Yelland et al., 1998).

location	x (m)	y (m)	z (m)
P (BIO sonic)	34.77	18.40	2.21
P _{stream}	34.77	18.40	1.99
P-P _{stream}	0.0	0.0	0.22
P _{origin}	254.27	17.66	1.99
P _{stream} -P _{origin}		$\Delta y=0.74$	

Table 1 The vertical displacement, Δy , of the flow to the BIO sonic site.

location	x (m)	y (m)	z (m)
P (BIO Young)	34.77	18.66	1.79
P _{stream}	34.77	18.67	1.99
P-P _{stream}	0.0	-0.01	-0.20
P _{origin}	254.17	17.98	1.99
P _{stream} -P _{origin}		$\Delta y=0.69$	

Table 2 The vertical displacement, Δy , of the flow to the BIO Young site.

location	x (m)	y (m)	z (m)
P (NOAA sonic)	35.17	18.78	1.06
P _{stream}	35.18	18.79	0.99
P-P _{stream}	-0.01	-0.01	0.07
P _{origin}	254.05	18.09	0.99
P _{stream} -P _{origin}		$\Delta y=0.70$	

Table 3 The vertical displacement, Δy , of the flow to the NOAA sonic site.

location	x (m)	y (m)	z (m)
P (Kiel sonic)	34.77	18.46	0.46
P _{stream}	34.78	18.47	-0.01
P-P _{stream}	-0.01	-0.01	0.47
P _{origin}	253.92	17.69	-0.01
P _{stream} -P _{origin}		$\Delta y=0.78$	

Table 4 The vertical displacement, Δy , of the flow to the Kiel sonic site.

location	x (m)	y (m)	z (m)
P (Fast temperature)	34.77	17.90	0.06
P _{stream}	34.77	17.94	-0.01
P-P _{stream}	0.0	-0.04	0.07
P _{origin}	253.90	17.18	-0.01
P _{stream} -P _{origin}		$\Delta y=0.76$	

Table 5 The vertical displacement, Δy , of the flow to the Fast temperature sensor.

3.c The free stream velocity

The estimates of the vertical displacement were used to obtain the free stream velocities for the instrument sites. The air parcel reaching the instrument will have originated at a height of $(y - \Delta y)$, and the free stream velocity is obtained at that height on the free stream profile. The velocity of the flow at the instrument site is then compared to this freestream velocity to give the wind speed error.

Figure 6 shows part of the free stream profile near the wind tunnel wall, directly abeam of the BIO sonic anemometer ($x=34.77$, $0 < y < 150$, $z=100$). This indicates a free stream velocity of 15.83 m/s at a height of 17.66 m. Free stream velocities were obtained for the other instrument sites in a similar fashion and the results are included in Table 6.

3.d The effect of flow distortion on the wind speed.

The free stream flow has small, predictable gradients and can be estimated accurately at any given point on the vertical profile. In contrast, the flow at an instrument site can suffer from severe distortion and correspondingly large gradients in the velocity field. In addition, it is not always possible to locate the centre of a computational cell on the exact instrument position (see Moat et al., 1996). For these reasons the velocity at the instrument site is estimated from lines of data extracted in all three directions. Figure 7 to 11 show the lines of data through the BIO sonic, BIO Young, NOAA sonic, Kiel sonic and Fast temperature sensor respectively. The results for the instruments are summarised in Table 6. The velocity error at the instrument site (of height y) is expressed as a percentage of the free stream velocity (at height $y - \Delta y$). A positive percentage error indicates that the flow at the instrument sites has been accelerated.

Figure 7 to 11 are also used to estimate the gradient of the velocity of the flow in all three directions. These rates of change of velocity provide an indication of the accuracy of the

velocity error estimate and of the severity of the flow distortion. The rates of change for the instruments are given in terms of change per cell and per metre in Table 7. The results for all the sites show very small rates of change which suggests that the effects of flow distortion are small. This is confirmed by the small angle of the flow to the horizontal; at all sites, the wind speed components suggested an angle of flow to the horizontal of about 2 degrees.

Instrument site	Velocity from each direction (m/s)	Average velocity (m/s)	Free stream velocity (m/s)	% Error
BIO sonic	15.690 (x)	15.695	15.831	-0.86
	15.706 (y)			
	15.690 (z)			
BIO Young	15.722 (x)	15.725	15.854	-0.82
	15.729 (y)			
	15.723 (z)			
NOAA sonic	15.723 (x)	15.727	15.861	-0.85
	15.736 (y)			
	15.723 (z)			
Kiel sonic	15.730 (x)	15.727	15.833	-0.67
	15.721 (y)			
	15.730 (z)			
Fast temperature	15.670 (x)	15.673	15.792	-0.75
	15.679 (y)			
	15.670 (z)			

Table 6 Percentage velocity error at the instrument sites on the lattice tower.

Instrument site	Velocity data line	Rate of change of velocity per metre (ms^{-1}/m)	Rate of change of velocity per cell ($\text{ms}^{-1}/\text{cell}$)
BIO sonic	along (x)	0.009	0.005
	up (y)	0.075	0.015
	across (z)	0.003	0.002
BIO Young	along (x)	0.014	0.004
	up (y)	0.076	0.030
	across (z)	0.007	0.001
NOAA sonic	along (x)	0.012	0.003
	up (y)	0.075	0.030
	across (z)	0.007	0.002
Kiel sonic	along (x)	0.010	0.005
	up (y)	0.076	0.030
	across (z)	0.003	0.001
Fast temperature	along (x)	0.007	0.003
	up (y)	0.075	0.029
	across (z)	0.000	0.000

Table 7 Rate of change of velocity close to the instrument sites on the lattice tower.

4. The air flow at the IMET foremast and bowmast instrument sites.

4.a The IMET instrument locations

This section summarises the results found for the IMET instrument sites on the foremast and bow mast (see Figure 1). The procedures used were the same as those for the instruments on the lattice tower (Section 3). The IMET instruments were;

1) a Young anemometer located on the starboard crossarm of the ship's foremast. The crossarm of the foremast was not included in the model of the ship geometry since the Young anemometer site was added in to the flow distortion study at a relatively late date. In addition, although the height of the crossarm (or "yardarm") was indicated on the ship plans, the length and diameter were not. The x and y coordinates of the Young could be estimated from the ship plans, whilst the distance of the instrument from the ship's centre line had to be estimated from photographs.

2) an anemometer and a temperature sensor mounted on the bow mast (the "operational meteorological mast") located in the ship's bows, forwards of the lattice tower. The temperature sensor was located on the port side of the bow mast, whilst the wind sensor was mounted on the centre line of the ship and projected 0.76 m in front of the bow mast. The bow mast was removed for the FASTEX and LabSea experiments and was therefore not included in the model geometry.

In the VECTIS coordinate system, the instrument locations were;

Foremast Young	x = 23.02 m	y (height) = 19.35 m	z = 1.37 m
Bow mast wind sensor	x = 42.38 m	y (height) = 16.00 m	z = 0.00 m
Bow mast temperature sensor	x = 41.61 m	y (height) = 15.40 m	z = -0.99 m

4.b The vertical displacement and velocity error

For the foremast Young anemometer the airflow is raised by 1.29 m from its original height before it reaches the anemometer location (Table 8). The airflow has been raised by 0.44 m for the bow mast wind sensor (Table 9) and by 0.53 m for the bow mast temperature sensor (Table 10).

Figures 12 to 14 show the lines of data through the foremast Young and bow mast wind and temperature sensors. The percentage velocity errors for these sites are summarised in Table 11. The rates of change of the velocity errors are shown in Table 12.

Although the rates of change for the foremast Young are small there is some uncertainty in the actual position of the instrument. Errors in the y and z direction of a few tens of centimetres could be possible. The bow mast instrument sites experience very small rates of change in velocity across the ship, but exhibit slightly larger rates of change in the vertical.

location	x (m)	y (m)	z (m)
P (foremast Young)	23.02	19.35	1.37
P _{stream}	23.01	19.32	0.99
P-P _{stream}	0.01	0.03	0.38
P _{origin}	254.02	18.03	0.99
P _{stream} -P _{origin}		$\Delta y=1.29$	

Table 8 The vertical displacement, Δy , of the flow to the foremast Young

location	x (m)	y (m)	z (m)
P (bow mast wind)	42.38	16.00	0.00
P _{stream}	42.38	16.00	-0.016
P-P _{stream}	0.00	0.00	0.016
P _{origin}	254.33	15.56	-0.016
P _{stream} -P _{origin}		$\Delta y=0.44$	

Table 9 The vertical displacement, Δy , of the flow to the bow mast wind sensor.

location	x (m)	y (m)	z (m)
P (bow mast temp.)	41.61	15.40	-0.99
P _{stream}	41.62	15.40	-1.01
P-P _{stream}	-0.01	0.00	0.02
P _{origin}	254.20	14.87	-1.01
P _{stream} -P _{origin}		$\Delta y=0.53$	

Table 10 The vertical displacement, Δy , of the flow to the bowmast temperature sensor.

Instrument site	Velocity from each direction (m/s)	Average velocity (m/s)	Free stream velocity (m/s)	% Error
foremast Young	16.004 (x)	16.028	15.871	0.99
	16.038 (y)			
	16.042 (z)			
bow mast wind	15.320 (x)	15.316	15.663	-2.30
	15.310 (y)			
	15.318 (z)			
bow mast temp.	15.271 (x)	15.273	15.600	-2.10
	15.279 (y)			
	15.268 (z)			

Table 11 Percentage velocity error at the IMET foremast and bowmast sites.

Instrument site	Velocity data line	Rate of change of velocity per metre (ms^{-1}/m)	Rate of change of velocity per cell ($\text{ms}^{-1}/\text{cell}$)
foremast Young	along (x)	0.029	0.059
	up (y)	0.077	0.023
	across (z)	0.121	0.033
bow mast wind	along (x)	0.048	0.044
	up (y)	0.101	0.071
	across (z)	0.000	0.000
bow mast temp.	along (x)	0.050	0.059
	up (y)	0.100	0.078
	across (z)	0.001	0.004

Table 12 Rate of change of velocity close to the IMET foremast and bowmast sites.

5. Summary

The distortion of the flow of air to instrument sites on the RV Knorr has been quantified for a 10 m wind speed of 15 m/s blowing directly over the bows of the ship. It should be noted that the effects of flow distortion can vary rapidly with a change in the relative wind direction (Yelland et al., 1998), i.e. these results are valid for a bow-on flow only. The distortion of the flow is that due to the ship's hull and superstructure only, since small scale structures (the structure of the lattice tower) and very local obstructions (the other instruments) could not be modelled.

The vertical displacement (Δy) of the flow was used to get an effective anemometer height ($y - \Delta y$), and the wind speed error relates the actual flow at the instrument site to the free stream flow at this effective height. This approach is required if, for example, the wind speed data from an anemometer is used to calculate the wind stress via the dissipation method (Yelland et al., 1998). The results for all the instruments sites are summarised in Table 13.

For the instrument sites on the lattice tower, the vertical displacement of the flow is relatively insensitive to the exact instrument location, varying by less than 10 cm for a 1 m change in instrument location (Tables 1 to 5). This, along with the small rates of change for the velocities (Table 7), suggests that the velocity errors calculated are also fairly robust. The largest source of error is likely to be in the extraction of the data: Table 7 shows that the maximum variation of the velocity from one cell to the next in the location of the instruments is 0.015 m/s for the BIO sonic and 0.03 m/s for the others. These figures, in the form of a percentage of the free stream flow, are indicated in brackets in Table 13. Given these limits, it can be seen that the results for the different instrument sites on the lattice tower do not differ significantly: all would be well represented by a deceleration of the flow by 0.8% and a vertical displacement of 0.75 m.

Compared to the lattice tower sites, the IMET instruments on the foremast and bow mast show similar rates of change per metre for the velocity error. However, the mesh density in these areas was not as high since the main region of interest was initially situated around the instruments on the lattice tower. The variable mesh density is illustrated in the figures in the Appendix. The larger cell sizes around the foremast and bow mast resulted in a

larger rate of change per cell, with maximum rates of change being of the order of 0.7 m/s, or about 0.4% of the freestream velocity for these instruments. The instruments on the bow mast both experience a deceleration of the flow of about 2% and a vertical displacement of the flow of about 0.5m. The flow to the site of the Young anemometer on the foremast is displaced upwards by 1.3m and accelerated by 1%, in contrast to the deceleration of the flow to all other instrument sites. In practice however, the Young on the foremast may well be affected by the wake from the lattice tower which is almost directly upwind of the Young.

Instrument	Instrument height, y. (m)	Velocity at instrument (m/s)	Free stream velocity (at $y - \Delta y$) (m/s)	% velocity error at instrument site	Vertical displacement Δy (m)	Angle of flow to the horizontal (degrees)
BIO sonic	18.40	15.695	15.831	-0.86 (0.10)	0.74 ± 0.10	2.4
BIO Young	18.66	15.725	15.854	-0.82 (0.19)	0.70 ± 0.10	2.3
NOAA sonic	18.78	15.727	15.861	-0.85 (0.19)	0.70 ± 0.10	2.3
Kiel sonic	18.46	15.727	15.833	-0.67 (0.19)	0.78 ± 0.10	2.3
Fast temperature	17.90	15.673	15.792	-0.75 (0.19)	0.76 ± 0.10	2.3
foremast Young	19.35	16.028	15.871	+0.99 (0.37)	1.29 ± 0.10	3.3
bow mast wind sensor	16.00	15.316	15.663	-2.30 (0.45)	0.44 ± 0.10	2.8
bow mast temp. sensor	15.40	15.273	15.600	-2.10 (0.50)	0.53 ± 0.10	3.0

Table 13. Summary of the results for all instrument sites on the RV Knorr. The figures in brackets indicate the maximum rate of change of velocity per cell (expressed as a percentage of the free stream velocity) for each site.

If data from the anemometer is used simply for measuring the mean wind speed, rather than the wind stress, then the use of an effective anemometer height is not essential and the freestream velocity can be obtained at the actual instrument height. For completeness, Table 14 shows the percentage velocity error for each instrument if the freestream velocity is calculated in this fashion.

Instrument	Instrument height, y (m)	Velocity at instrument (m/s)	Free stream velocity at height y (m/s)	% velocity error at instrument site
BIO sonic	18.40	15.695	15.885	-1.20
BIO Young	18.66	15.725	15.905	-1.13
NOAA sonic	18.78	15.727	15.914	-1.18
Kiel sonic	18.46	15.727	15.890	-1.03
Fast temperature	17.90	15.673	15.848	-1.10
foremast Young	19.35	16.028	15.964	+0.40
bow mast wind sensor	16.00	15.316	15.695	-2.41
bow mast temp. sensor	15.40	15.273	15.644	-2.37

Table 14. The wind speed error calculated using a freestream velocity at the actual instrument height, y .

6. Acknowledgements

This work was supported by funds from the University of Kiel (Germany), Bedford Institute of Oceanography (Nova Scotia) and from NOAA and the Naval Postgraduate School (USA).

7. References

- Moat, B. I. and M. J. Yelland, 1998: Air-flow over the RV Knorr: a numerical model of the ship. Unpublished contract report.
- Moat, B. I., M. J. Yelland and J. Hutchings, 1996: Airflow over the R.R.S. Discovery using the Computational Fluid Dynamics package Vectis, SOC Internal report 2, Southampton Oceanography Centre, Southampton, UK.

Yelland, M. J., B. I. Moat, P. K. Taylor, R. W. Pascal, J. Hutchings and V. C. Cornell, 1998: Wind stress measurements from the open ocean corrected for airflow distortion by the ship. *J. Phys. Oceanogr.*, **28** (7), 1511--1526.

8. Figures

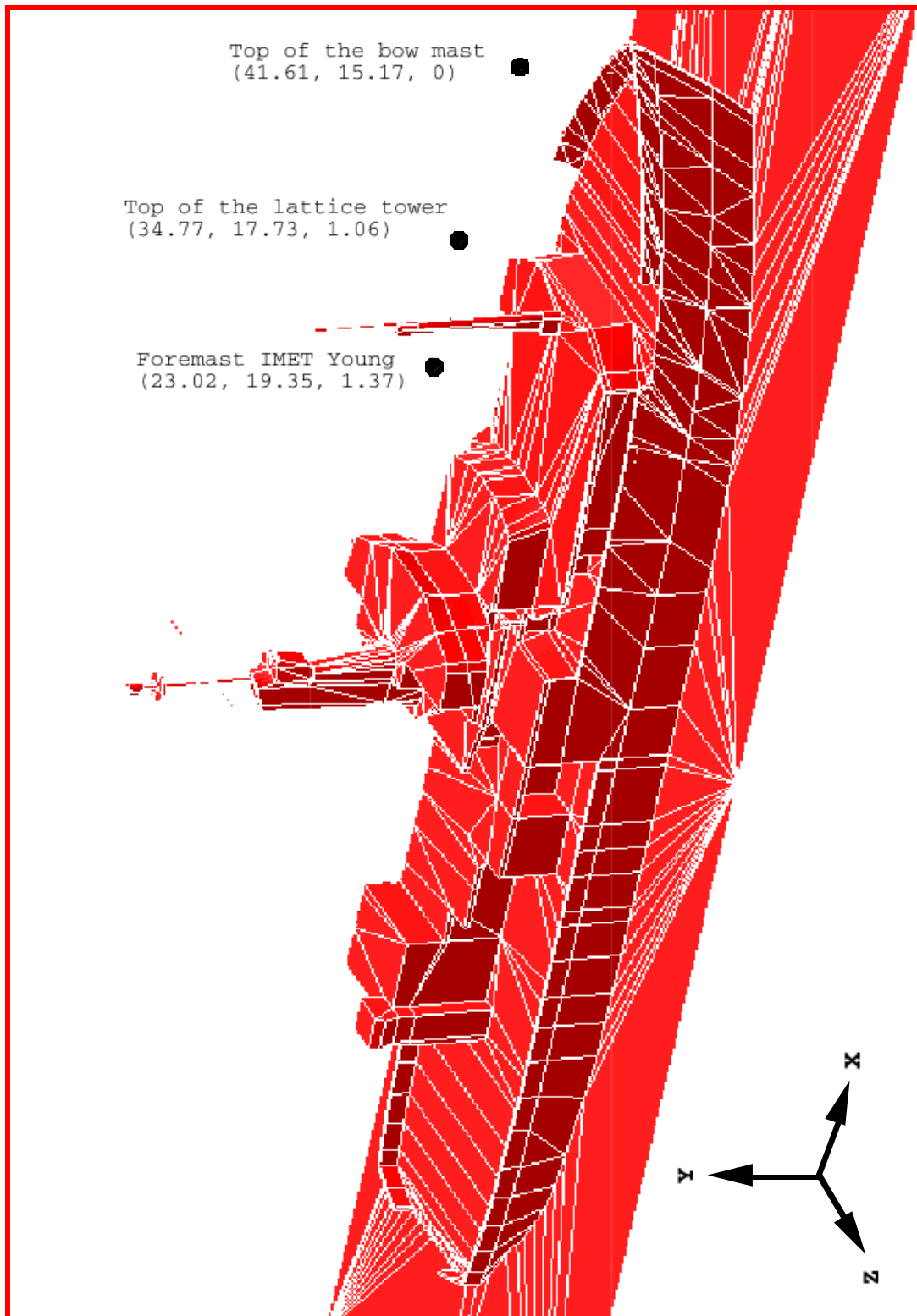


FIGURE 1 A 3dimensional view of the model of the RV Knorr. The position of the top of the bow mast, the lattice tower and the foremast instrument sites are indicated, and their x, y, z coordinates are given in brackets.

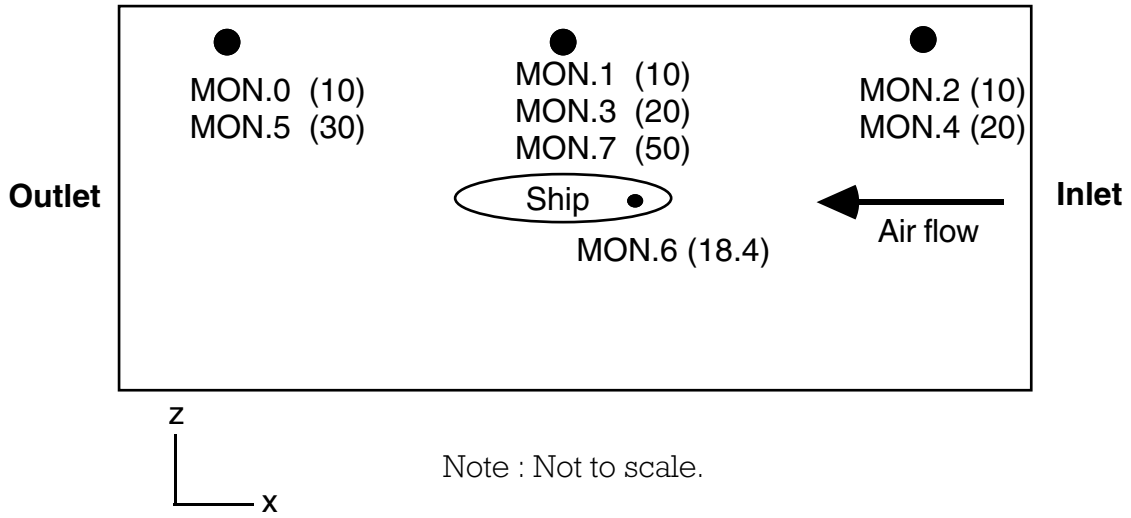


Figure 2. Schematic plan view of the "wind tunnel" used to simulate a flow of air over the bows of the RV Knorr. The monitoring positions are shown by the solid circles and their heights in metres are indicated in brackets.

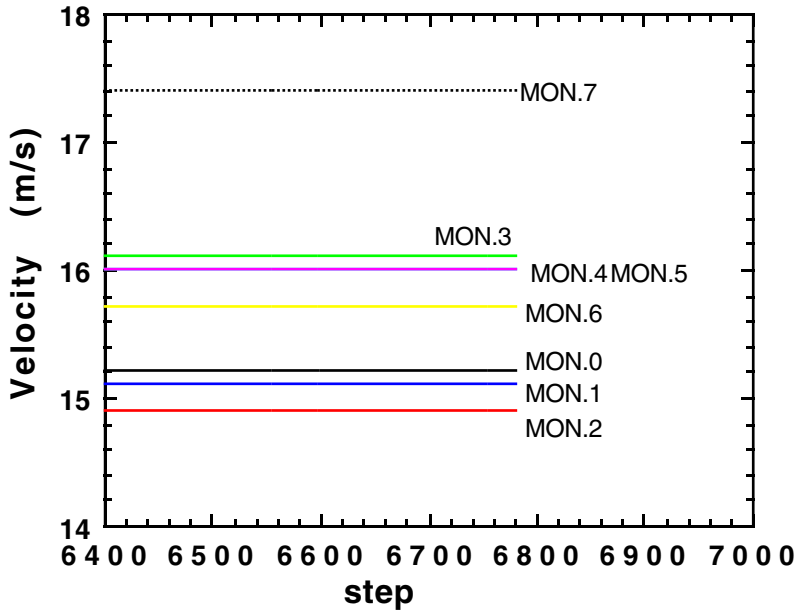


Figure 3. Velocity data from the eight monitoring locations, for the last 300 time steps.

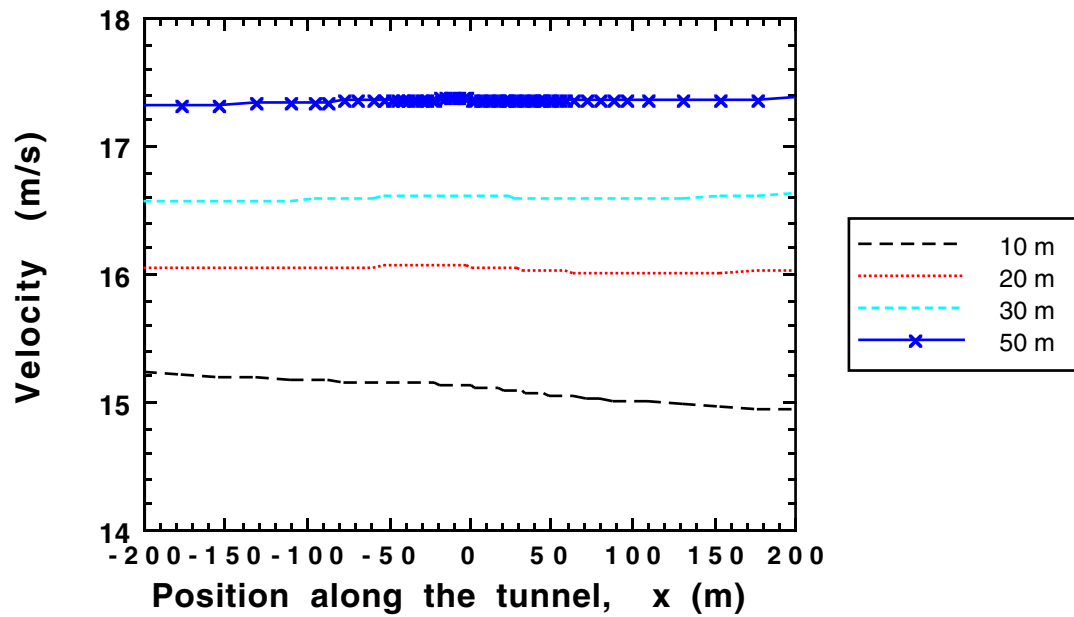


Figure 4a. Lines of velocity data along the length of the tunnel at the heights shown. The data were obtained from the free stream region towards one side of the tunnel.

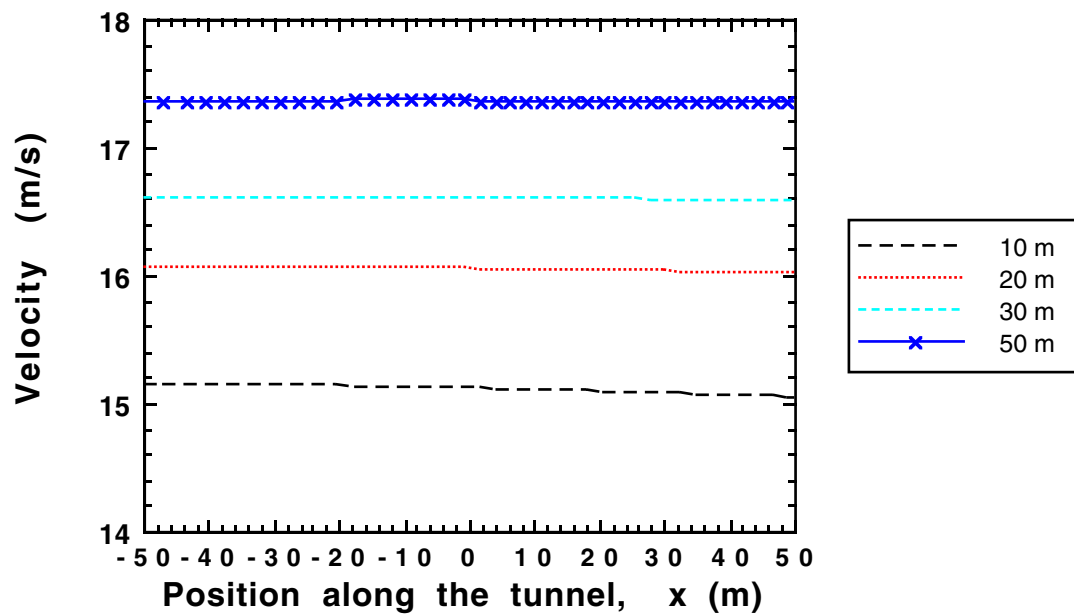
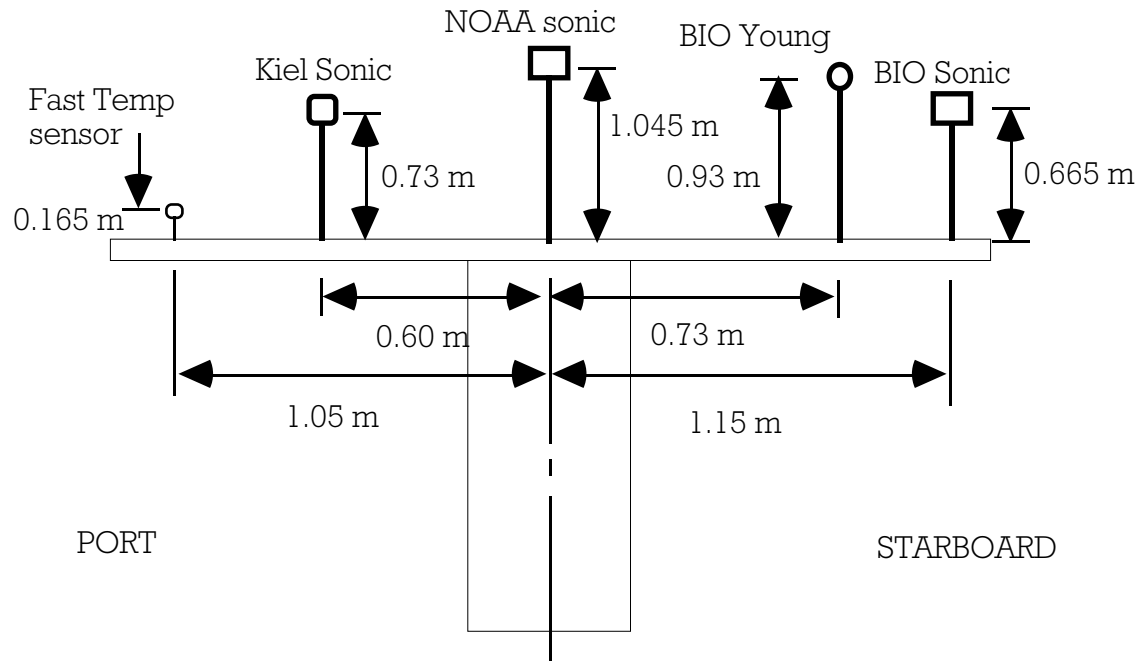
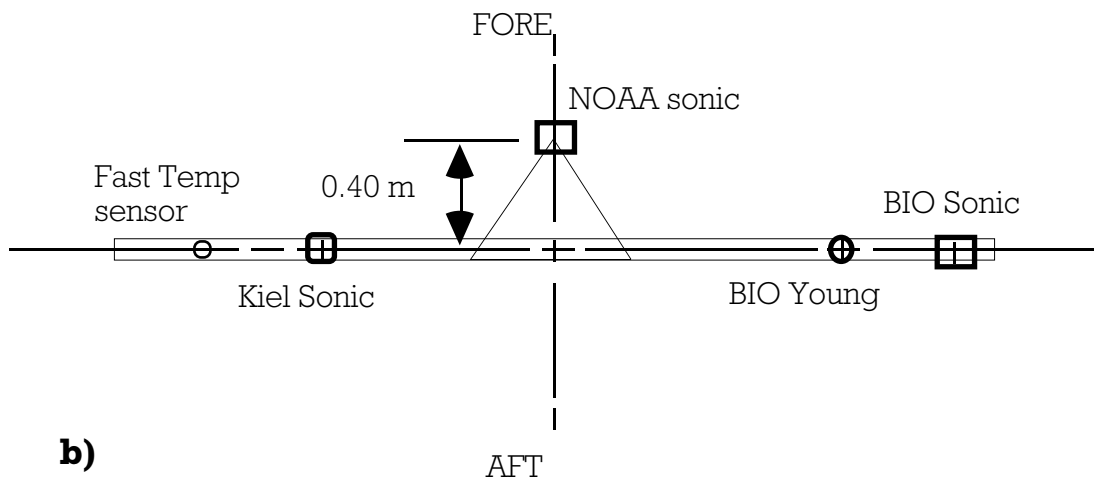


Figure 4b. As 4a, showing the central portion of the tunnel only.



a)



b)

Figure 5 Schematic of the instrument positions relative to the lattice tower in the bows of the RV Knorr; a) viewed from astern, b) plan view. N.B. The tower itself is not modelled.

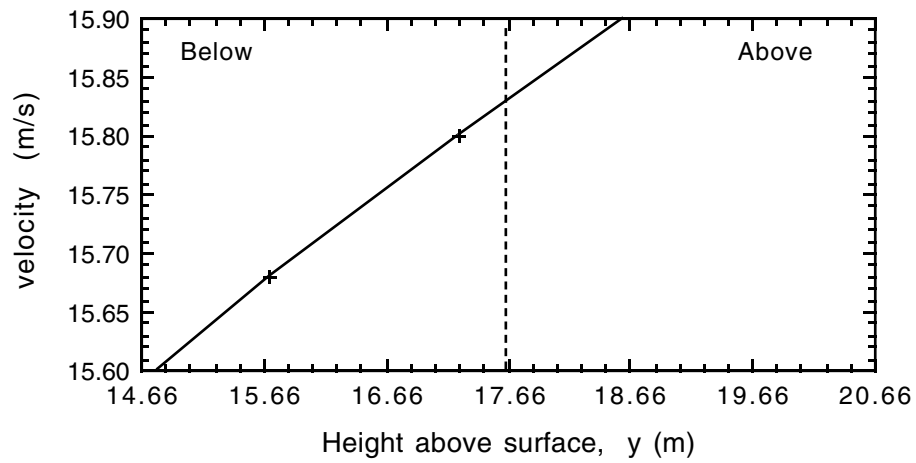


Figure 6 The vertical profile of velocity abeam of the BIO sonic anemometer site. The dashed line indicates the height from which the air flow originated.

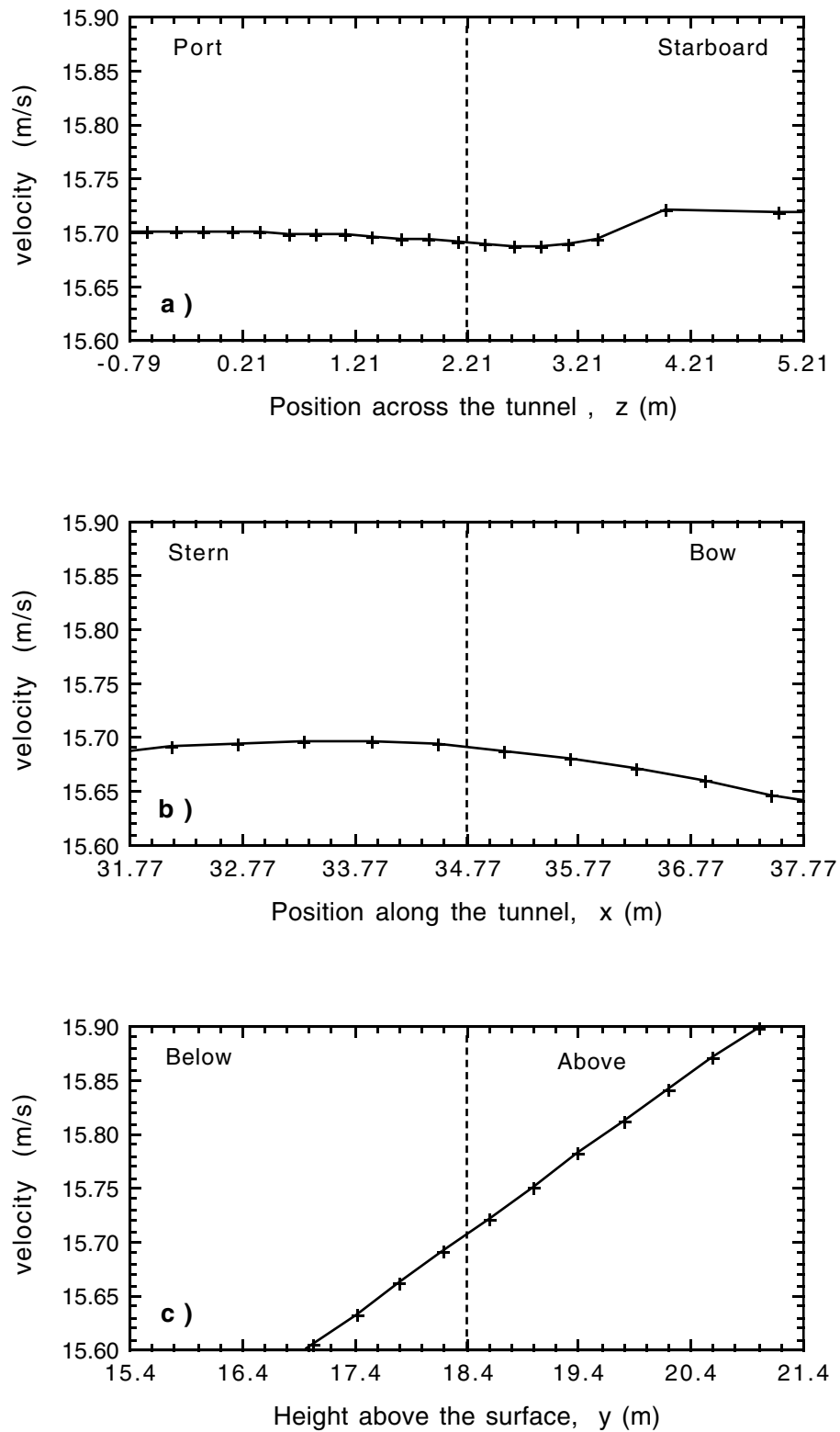


Figure 7 Lines of velocity data through the BIO sonic position (indicated by the dashed line) in all three directions; a) across the tunnel, b) along the tunnel and c) vertically.

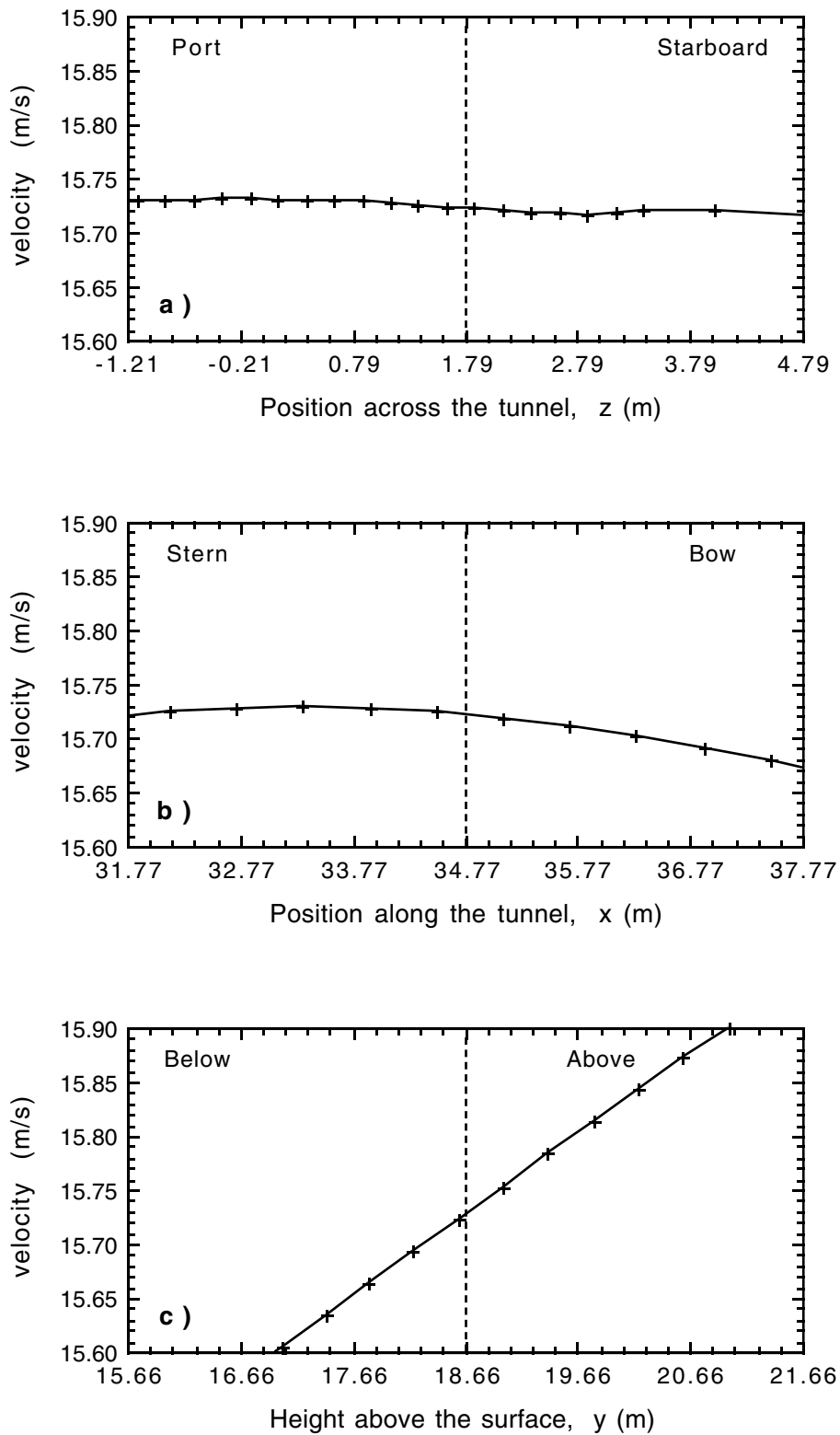


Figure 8 As for Figure 7 but for the BIO Young anemometer site.

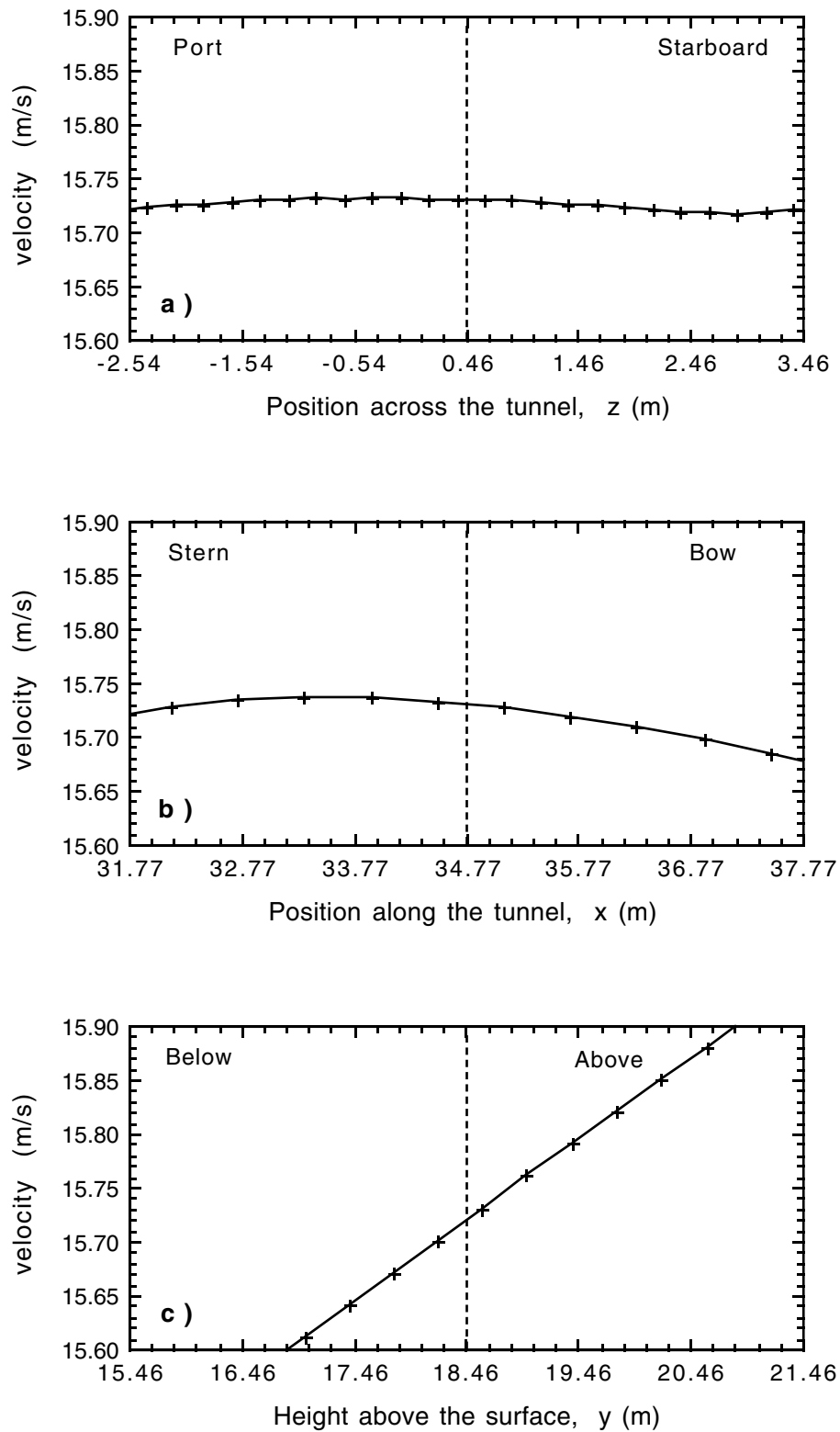


Figure 9 As for Figure 7 but for the Kiel sonic anemometer site.

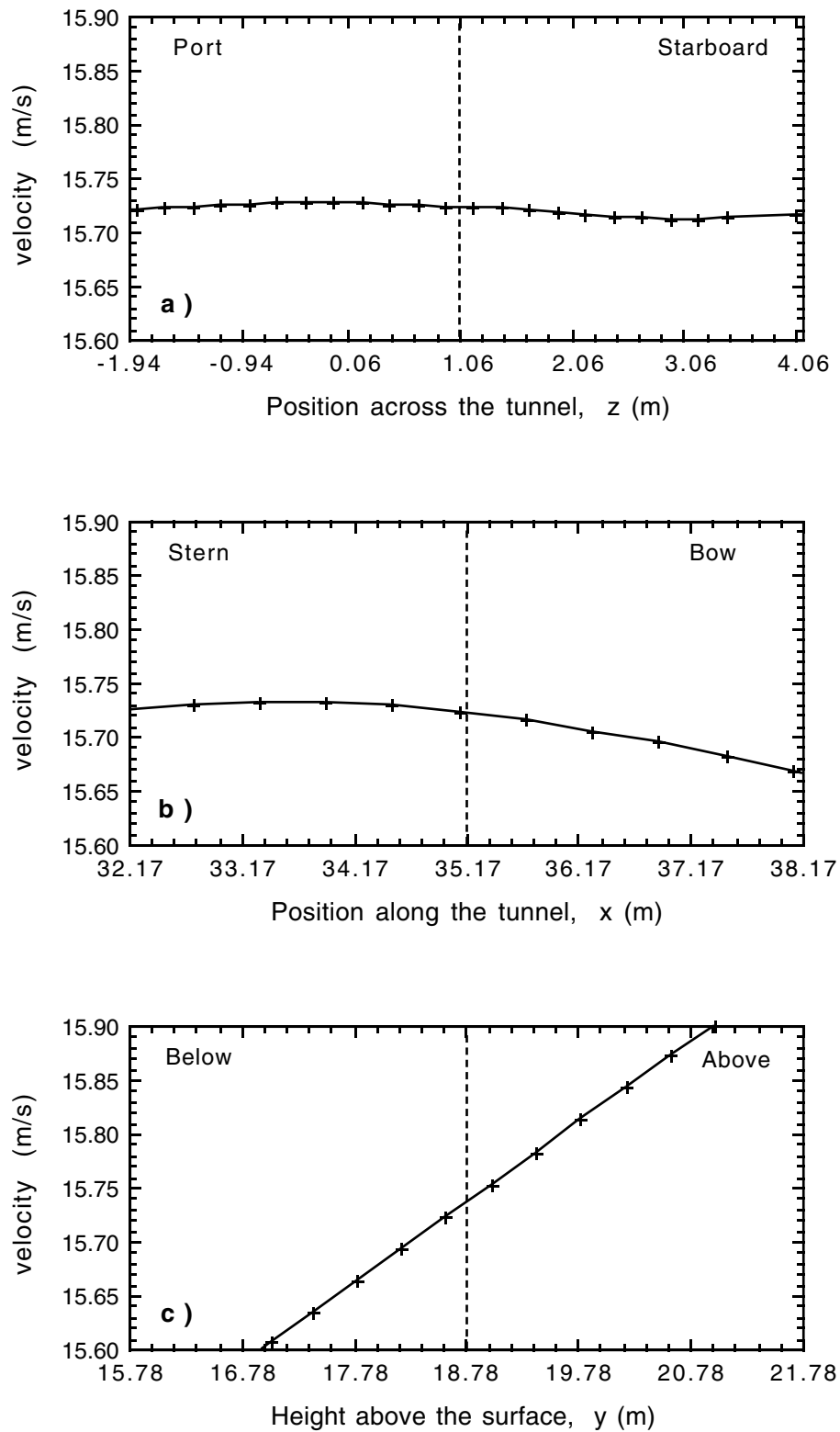


Figure 10 As for Figure 7 but for the NOAA sonic anemometer site.

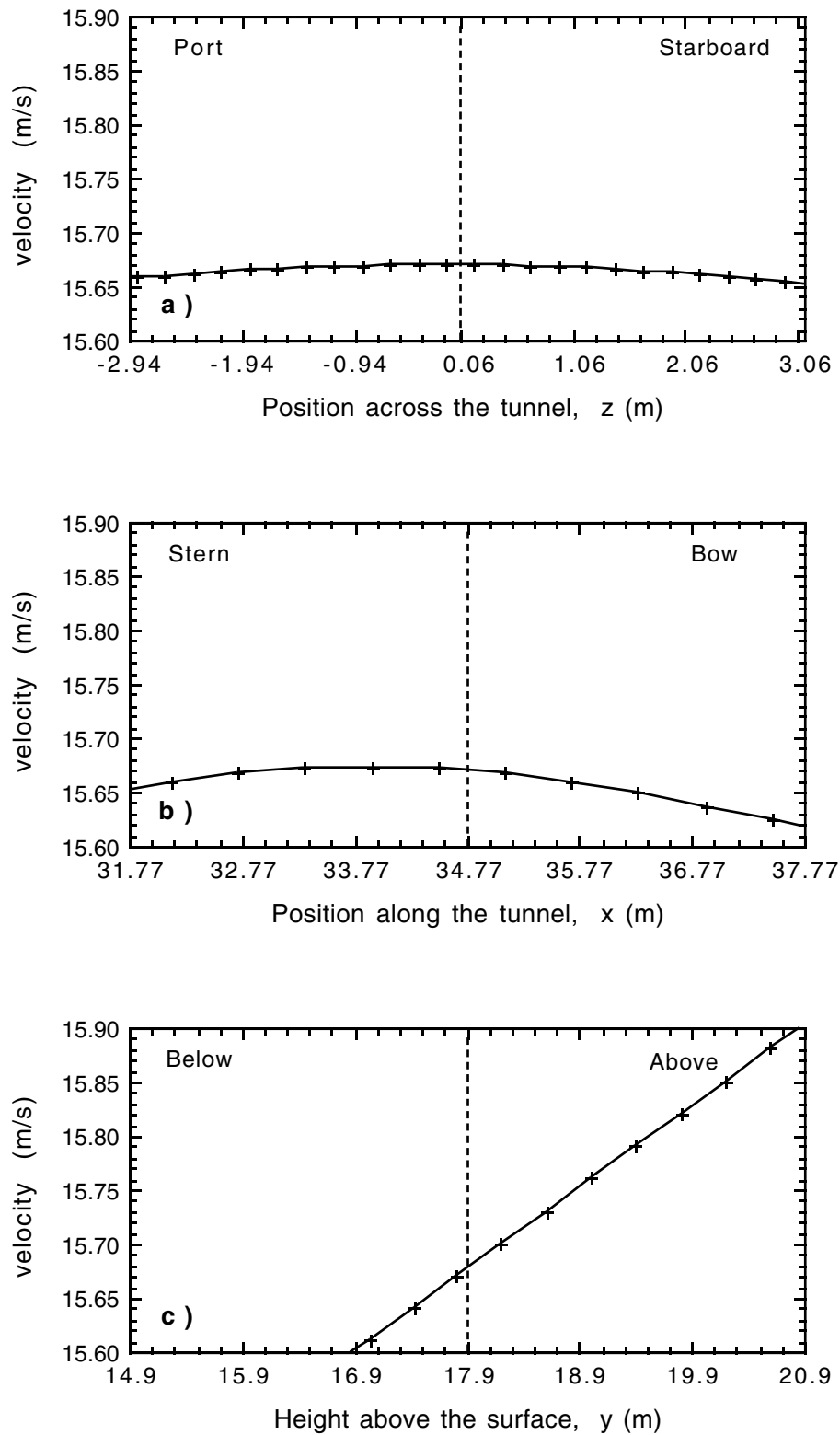


Figure 11 As for Figure 7 but for the fast temperature sensor site.

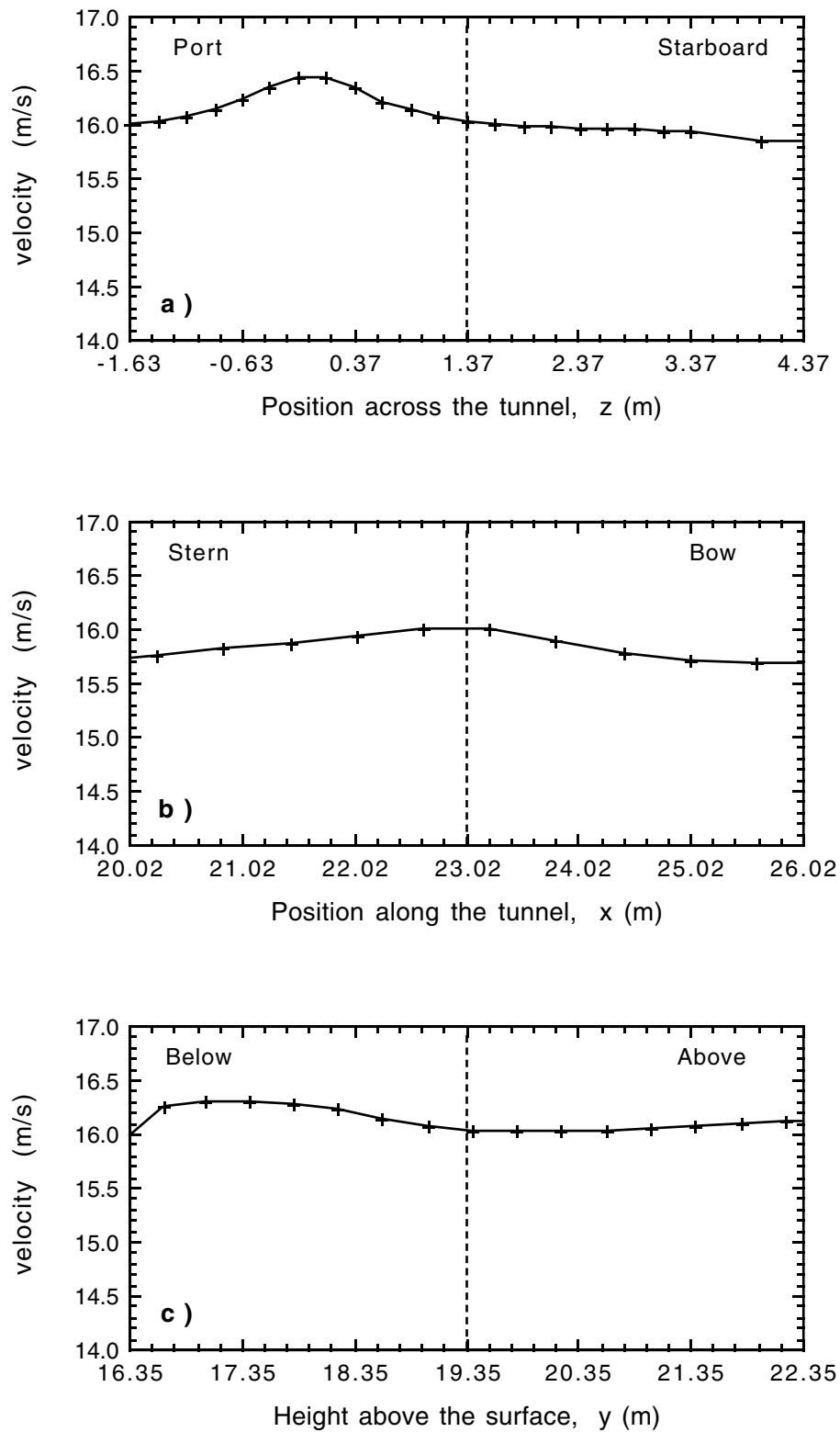


Figure 12 As for Figure 7 but for the IMET Young on the foremast.

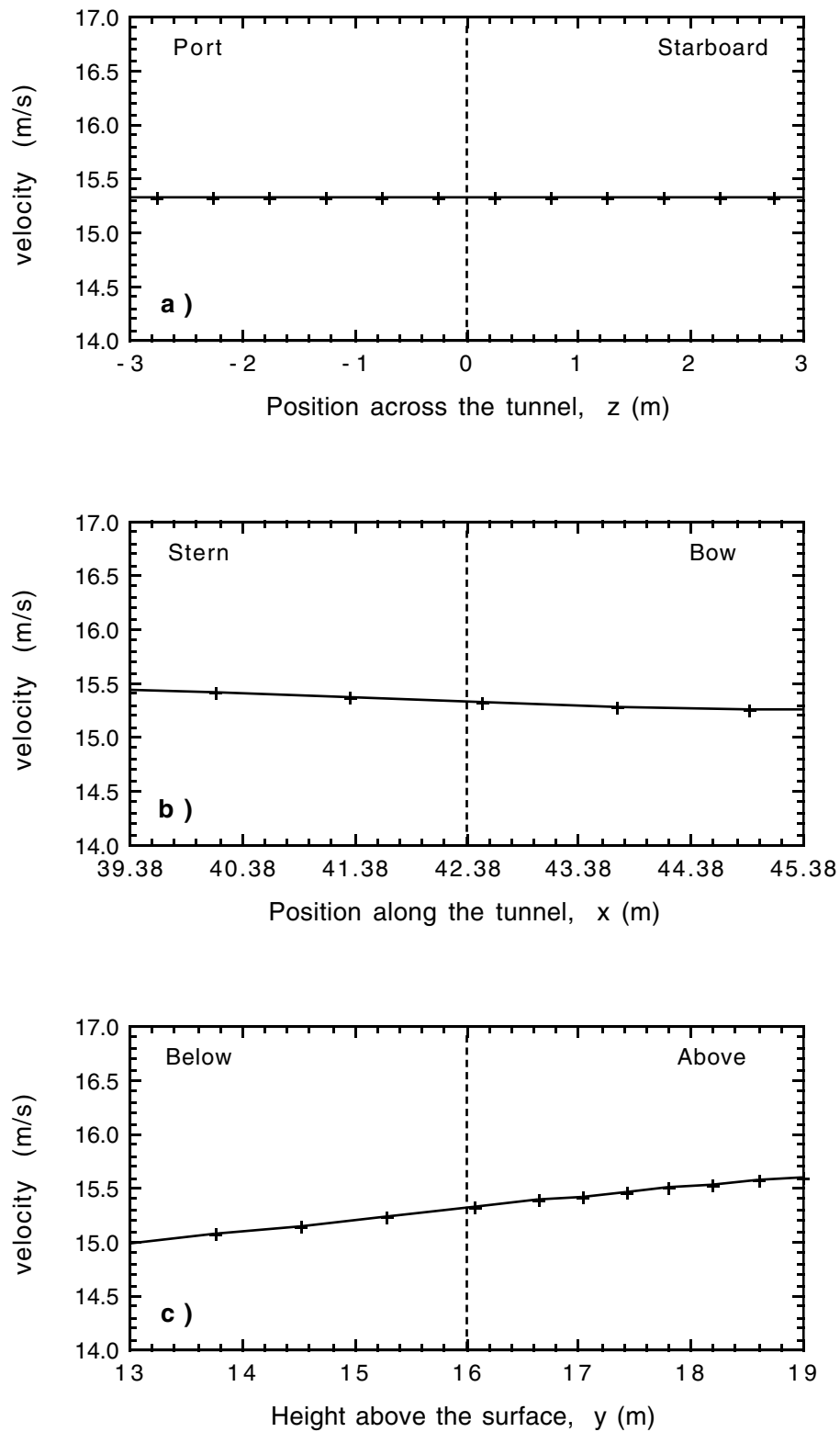


Figure 13 As for Figure 7 but for the IMET wind sensor on the bow mast.

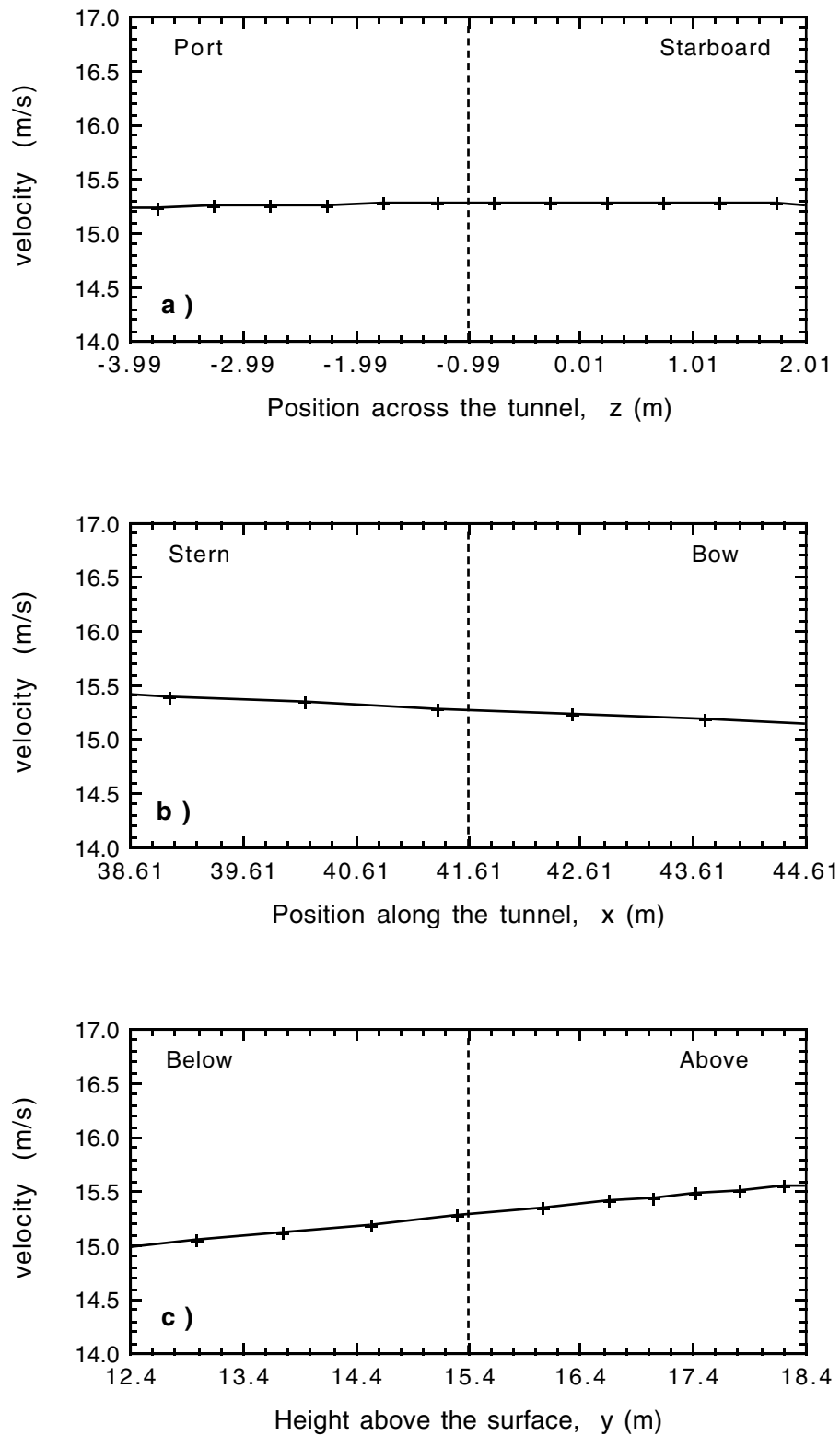


Figure 14 As for Figure 7 but for the IMET temperature sensor on the bow mast.

9. Appendix

The Figures in this Appendix were generated using the VECTIS post-processing software. Each Figure shows data on a major plane, and the orientation of the plane is indicated by the red line in the small box at the top left of each Figure. The variable size of the computational cells can be clearly seen in all the Figures.

Figure A1 Velocity vectors on a vertical plane through the centre line of the ship. The magnitude of the total velocity is indicated by the colour of the arrows. The length and direction of the arrows represent the magnitude and direction of the component of the velocity in the plane of view. Each arrow represents the result from one computational cell. The velocity scale corresponds to 13 m/s to 18 m/s. The position of the top of the bow mast and the site of the fast response temperature sensor are indicated by the crosses.

Figure A2 As Figure A1 for a vertical plane through the NOAA sonic anemometer site (indicated by the cross).

Figure A3 As Figure A1 for a vertical section across the tunnel which intersects the NOAA anemometer site (indicated by the cross).

Figure A4 As Figure A1 for a horizontal section through the NOAA sonic anemometer site (indicated by the cross).

Figure A5 A streamline, or massless particle trace, which passes through the NOAA sonic anemometer site (indicated by the cross).

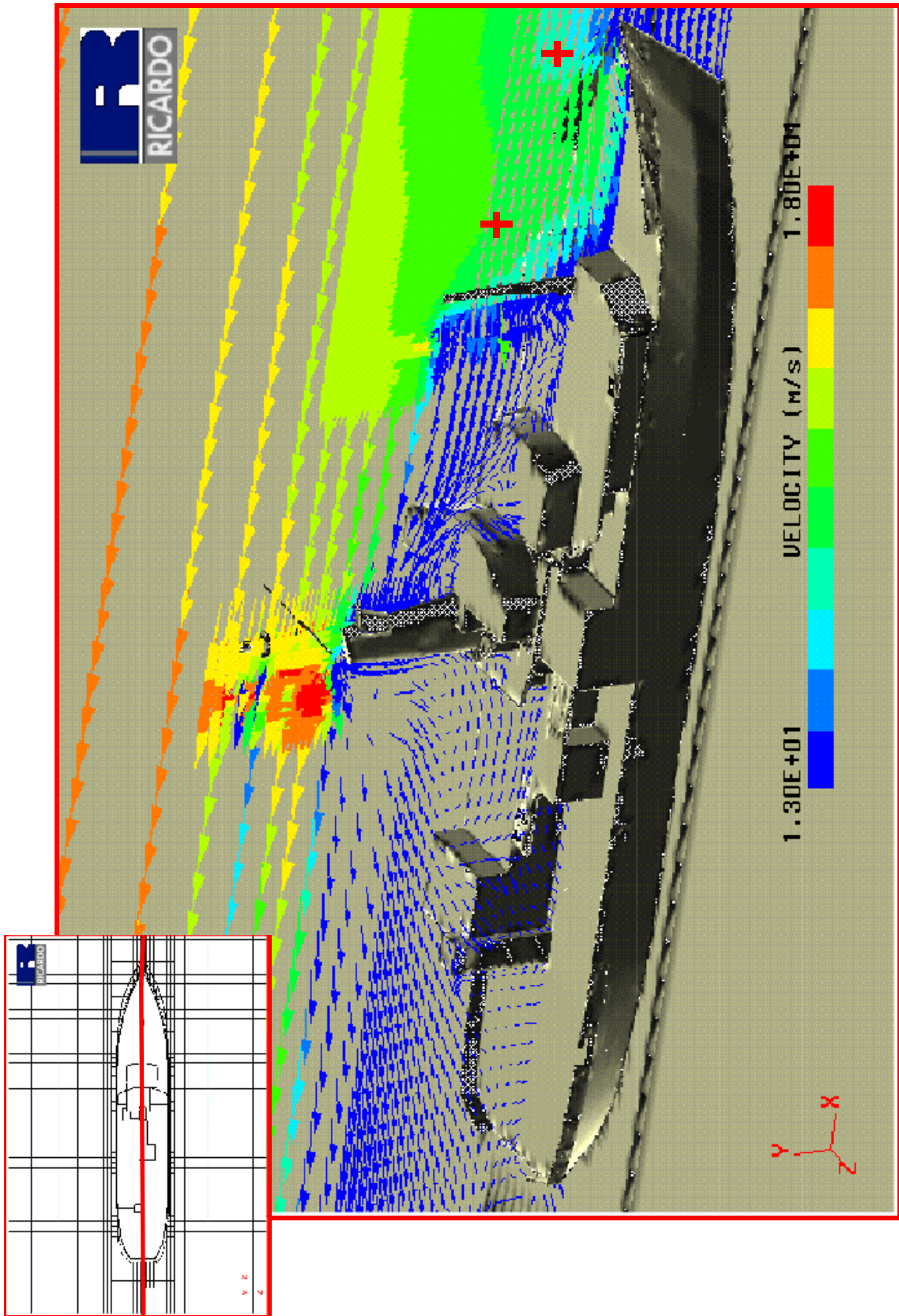


Figure A1

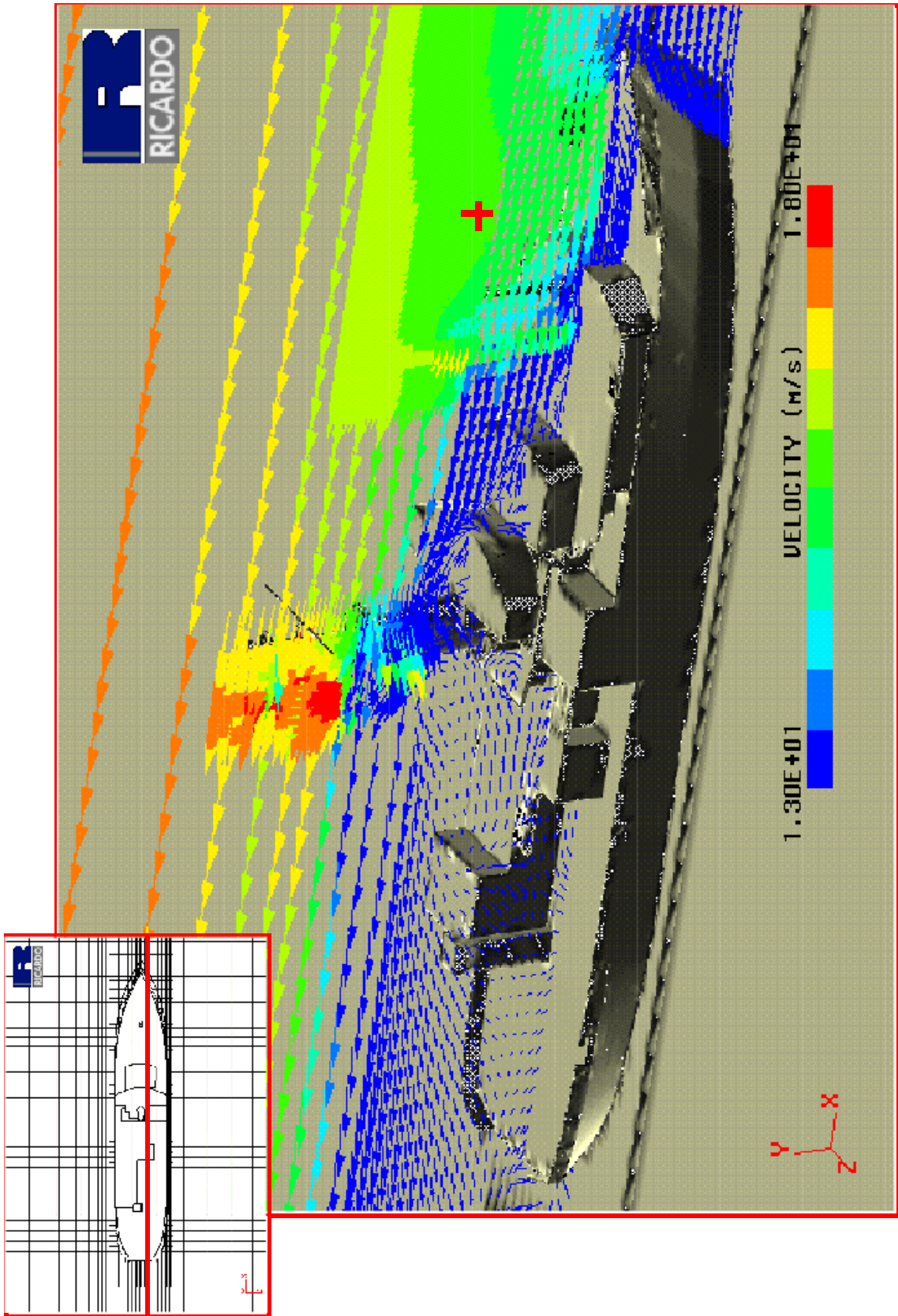


Figure A2

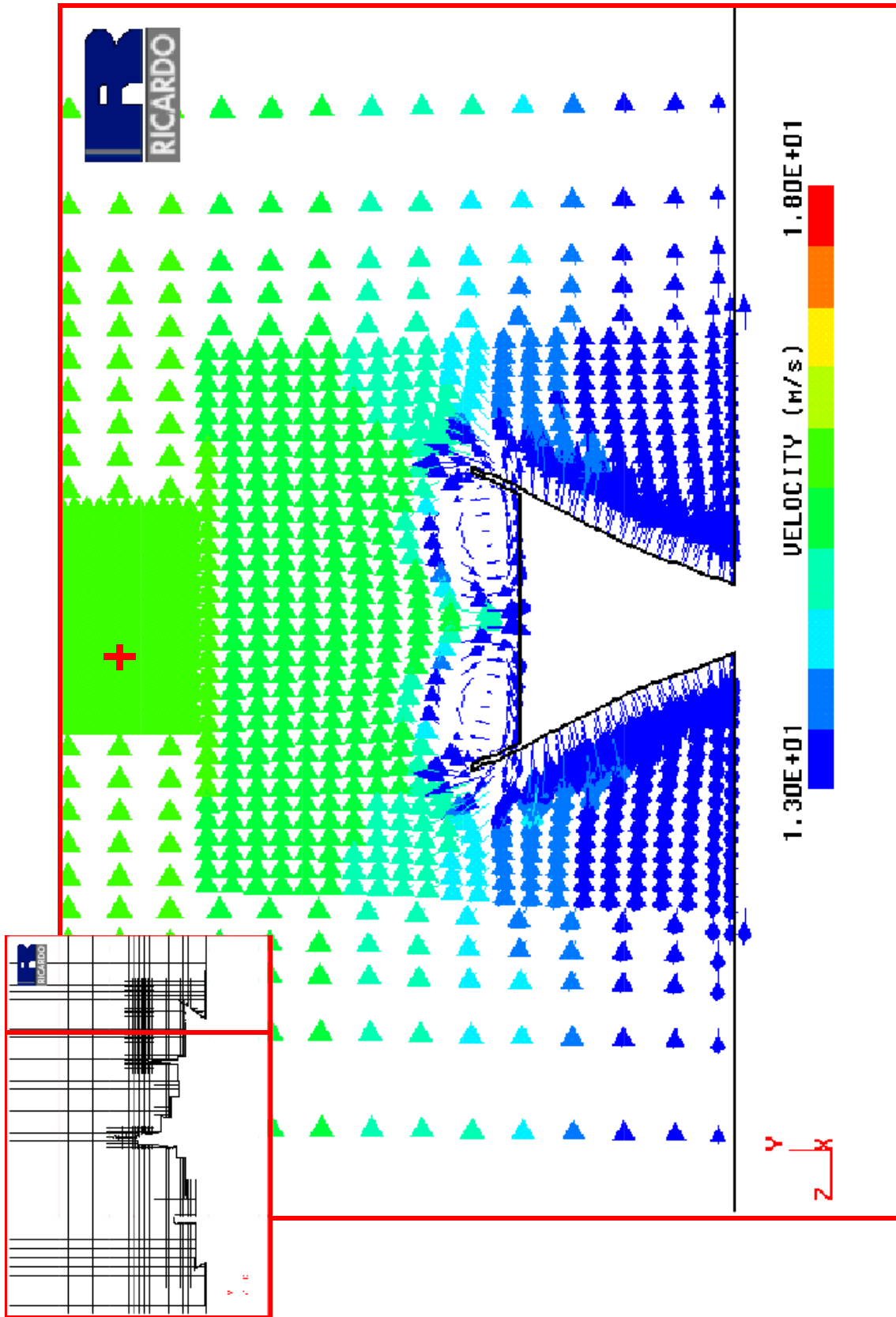


Figure A3

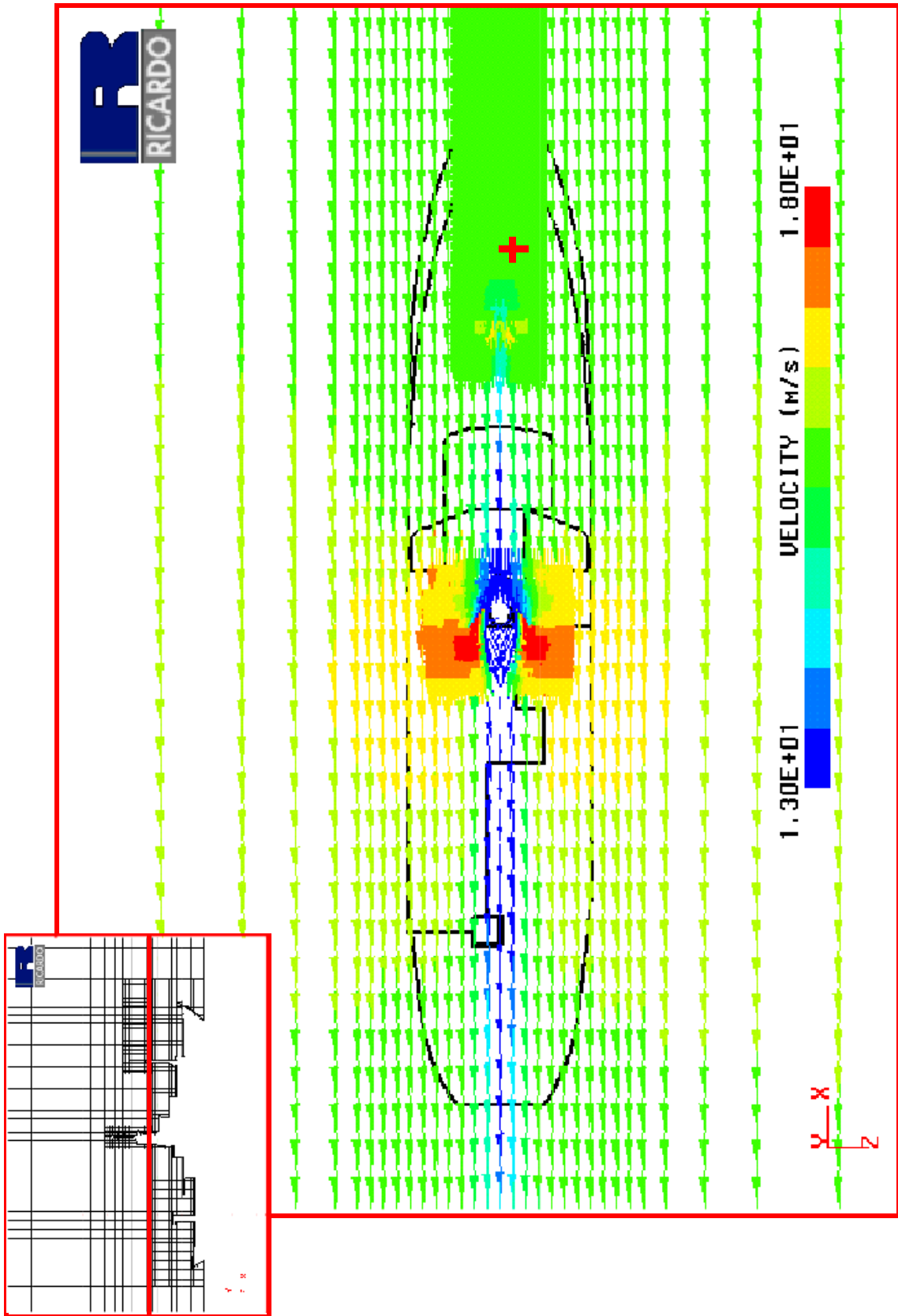


Figure A4

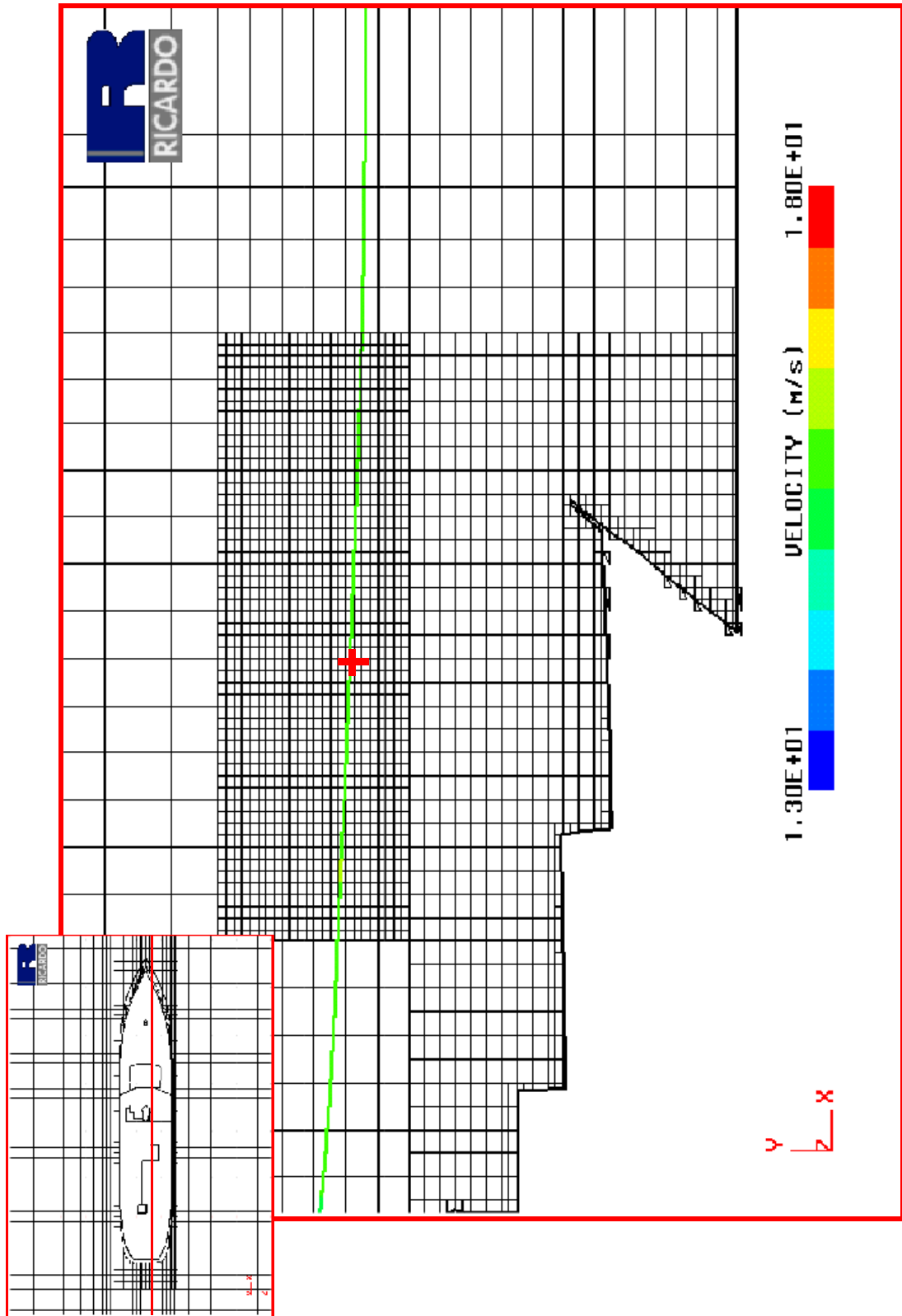


Figure A5